Theory of Morphological Transitions in Weakly Dissociating Diblock Polyelectrolyte Micelles

E. B. Zhulina[†,‡] and O. V. Borisov[*,†,‡]

Institute of Macromolecular Compounds of the Russian Academy of Sciences, 199004, St. Petersburg, Russia, and DRFMC/SI3M, CEA-Grenoble, 38000 Grenoble, France

Received March 26, 2005

ABSTRACT: We present a theory that describes equilibrium morphologies of micelles formed by diblock copolymer with one neutral and one weakly dissociating polyelectrolyte block in dilute aqueous solution. We demonstrate that, depending on the copolymer composition, variations in the pH and the ionic strength in the solution can trigger different sequences of morphological transitions. At high solution salinity, an increase in ionic strength gives rise to sphere-to-cylinder and cylinder-to-lamella transitions. At low solution salinity, the sequence of morphological transformations is reversed, and micelles undergo lamella-to-cylinder and cylinder-to-sphere transitions upon an increase in the salt concentration. We obtain the diagrams of states of diblock copolymer solution and derive analytical expressions for binodal lines corresponding to the first-order phase transitions and the coexistence of aggregates of different morphologies. Our results provide the guidelines to create block polyelectrolytes aggregates with stimuli-induced polymorphism.

1. Introduction

Amphiphilic molecules are known to associate into micelles (finite size aggregates) and mesophases in aqueous media.[1,2] The aggregates of amphiphilic ionic macromolecules are extensively explored for the potential applications in nanotechnology, controlled encapsulation, delivery and release of drugs, agrochemicals, etc. A number of experimental[3−15] and theoretical[16−22] studies were carried out to understand the self-assembly of ionic polymeric amphiphiles in the solution.

In the case of diblock copolymer with one hydrophobic and one polyelectrolyte block the structure and equilibrium morphology of a micelle are determined by the balance of the hydrophobic attraction between the insoluble blocks and the Coulomb repulsion between the hydrophilic (ionic) blocks. The latter can be tuned by variations in the ionic strength of the solution due to screening of the electrostatic interactions by added salt. An increase in the salinity leads to the decrease in specific area of the hydrophobic core per molecule and can cause a succession of transitions from the spherical (S) to cylindrical (C) micelles and further to the lamellar (L) aggregates. The driving force for such morphological transitions is the same as for neutral polymeric amphiphiles.[23,24] It is the increase in conformational entropy of the extended nonionic block in the hydrophobic domain in the row S−C−L. Recent experimental studies on solutions of symmetric diblock copolymer with strongly dissociating polyelectrolyte block demonstrated the existence of aggregates with different morphologies (see ref 15 for a review). The results are in qualitative agreement with the theoretical predictions.[20,22]

A novel domain in the micelle behavior arises when the polyelectrolyte block is weakly dissociating (pH-sensitive), i.e., constitutes a weak polyacid or polybase. For such polyamphiphiles there is a strong coupling between the aggregation and ionization of the coronal blocks. As a result, the response of the system to variations in the solution salinity is more complicated than that for a copolymer with strongly dissociating polyelectrolyte block. Our analysis[21] indicates that a diblock copolymer with a relatively long pH-sensitive block can associate into starlike spherical micelles. Because of the ionization/association coupling, two types of aggregates are possible: large micelles with strongly suppressed corona ionization (referred to as quasi-neutral micelles) and small micelles with strongly ionized corona (referred to as charged micelles). The quasi-neutral micelle with acidic corona is thermodynamically stable at relatively small ionic strength and low pH in the solution whereas the charged micelle is found at larger ionic strength or/and high pH. The aggregates with intermediate aggregation numbers and degrees of corona ionization are thermodynamically unstable. An increase in solution salinity or pH triggers the abrupt transformation of a large quasi-neutral micelle into several smaller charged micelles. This scenario takes place in a narrow range of the pH values that is determined by the molecular weights of the blocks. Outside of this range, an increase in solution salinity leads to gradual rearrangement of the spherical micelle.

The self-consistent-field numerical calculations were performed recently[25] to probe the structure of a spherical micelle with pH-sensitive corona. Two populations of spherical micelles were detected: large weakly charged and small strongly charged micelles. In agreement with our prediction, the transformation of a large weakly charged micelle into smaller strongly charged micelles occurred as the first-order phase transition. The nonmonotonic behavior of micelle characteristics as a function of salt concentration was also confirmed.

Diblock copolymer with shorter hydrophilic (ionizable) block associates in the so-called crew cut micelles with corona thickness smaller than the core size. Spherical crew cut micelles can also undergo abrupt transformations: large weakly ionized crew cut aggregates can transform into small strongly charged starlike micelles.

[†] Institute of Macromolecular Compounds of the Russian Academy of Sciences.
[‡] CEA-Grenoble.

10.1021/ma050634w CCC: $30.25
Published on Web 06/17/2005

However, in contrast to starlike micelles, spherical crew cut micelles can have intermediate degrees of corona ionization in response to variations in the solution salinity.[21] For the crew cut micelles, the conformation entropy of the extended core blocks becomes important. To reduce the extension of the core blocks and thus gain the conformational entropy, micelles can also change their morphology upon variations in the salinity of solution.

In our previous study[22] of the morphological transitions in aggregates of ionic polyamphiphiles, we focused on the case of relatively large ionic strength in solution. Under those conditions the degree of corona ionization is controlled solely by the pH and is virtually independent of the solution salinity and aggregation state of the copolymer molecules. The electrostatic interactions in the corona are progressively screened upon an increase in the ionic strength. As a result, the morphological transformations in the crew cut aggregates, S−C−L, can take place. The general features of these transitions are similar to those for neutral diblock copolymers with variable solvent strength for solvophilic block.

The situation becomes dramatically different at low ionic strength in the solution. Under these conditions, the degree of corona ionization is governed by both, the pH and salinity in the solution, and increases with an increase in the ionic strength.

In our recent letter[26] we reported on possibility of the "reversed" sequence of morphological transitions, L−C−S, upon an increase in the ionic strength. This series of transitions is the unique manifestation of the annealing polyelectrolyte nature of micelle corona. Such transformations are not possible for diblock copolymer with strongly dissociating (quenched) polyelectrolyte block.

In this paper, we present a comprehensive theoretical description of the equilibrium structure and morphological transitions between the aggregates with pH-sensitive (weak polyacid) corona. Our aim is to establish the relationship between the copolymer composition (molecular weights of the blocks) and the structure of the phase diagram of the solution. We examine how the copolymer composition is related to the spectrum of equilibrium aggregate morphologies and sequences of possible morphological transitions. In contrast to the previously used model,[22] we take into account the inhomogeneous structure (polymer density gradient) in the corona and explicitely calculate the transition lines (binodals).

The rest of the paper is organized as follows. In section 2, we formulate the model of a micelle with pH-sensitive corona. In section 3, we describe the general formalism to describe micelles of different morphology. In section 4, the starlike spherical micelles are described. We briefly summarize there our predictions[22] on the phase S−S transition between spherical micelles with strongly and weakly ionized coronas. In section 5, we analyze the crew cut micelles of different morphologies and examine sequences of morphological transitions that take place at low and high salt concentrations in the solution. In section 6, we construct the phase diagrams of diblock copolymer solution. Finally, in section 7, we summarize the conclusions.

2. Model

We consider a dilute aqueous solution of block copolymer comprising a hydrophobic block with degree of polymerization N_B and a weak polyacid block with degree of polymerization N_A. Each monomer of the polyacid can be ionized via dissociation of hydrogen ion, H^+. (For polybases, ionization occurs through protonation of the monomer, and generalization of the model is straightforward). The dissociation constant for the acidic monomer is K. The degree of dissociation of the acidic monomer in the bulk of the solution, α_b, depends on the value of pH (the bulk concentration c_{bH^+} of H^+ ions) via the mass action law,

$$\frac{\alpha_b}{1-\alpha_b} = \frac{K}{c_{bH^+}} \tag{1}$$

The solution contains also monovalent ions of various types due to added salt, base or acid.

Both blocks of copolymer are assumed to be flexible. That is, the statistical segment length is on the order of a monomer size a, which is taken as the unit length in our subsequent analysis. We assume also that the monomer size a is on the order of the Bjerrum length, $l_B \simeq a$.

The short-range (van der Waals) interactions between monomers are modeled in terms of the virial expansion. In our subsequent analysis we focus on the case of relatively dilute systems. Here, only the pair monomer−monomer interactions with second virial coefficients $v_A a^3$ and $v_B a^3$ or the ternary interactions with third virial coefficients $w_A a^6$ and $w_B a^6$ are relevant. We assume that the value of v_A does not depend on the degree of dissociation and is the same (water is assumed to be a marginal good solvent, $v_A \geq 0$) for an ionized and nonionized monomer A. On the contrary, water is a poor solvent for hydrophobic block B, the value of dimensionless second virial coefficient v_B is negative, $v_B \cong (\Theta_B - T)/\Theta_B \cong -\tau \leq 0$ where Θ_B is the Θ-temperature for block B.

When the polymer concentration in solution exceeds the critical micelle concentration (*cmc*), diblock copolymer chains associate to form micelles. A micelle consists of the hydrophobic core comprising condensed blocks B that is surrounded by the polyelectrolyte corona of blocks A, Figure 1. We assume that the width of the core/corona boundary is small compared to the size of the micelle. Therefore, blocks A and B can be envisioned as tethered to the core/corona interface. The morphology of micelle is specified by index i. We consider here spherical ($i = 3$), cylindrical ($i = 2$) or lamellar-like ($i = 1$) micelles.

Below we consider the dilute polymer solution where the interactions between aggregates are weak and do not affect the structure of micelle.

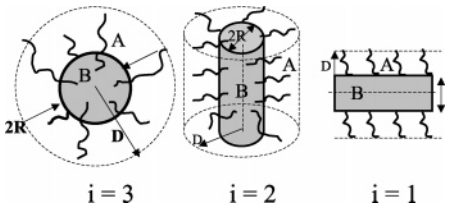

Figure 1. Self-assembled block copolymer aggregates of different morphologies: spherical ($i = 3$), cylindrical ($i = 2$), and lamellar ($i = 1$). Hydrophobic blocks B and polyelectrolyte blocks A form the core and the corona of aggregate, respectively.

3. General Formalism

The equilibrium structure and the free energy F per chain in the micelle are determined by the balance of

the excess free energy of the core/corona interface, $F_{\text{interface}}$, and the free energies of the core, F_{core}, and of the corona, F_{corona}.

To calculate the free energies and to analyze the equilibrium morphology of micelles, we generalize the model used in ref 23 to describe a neutral block copolymer micelle in a selective solvent. The polyelectrolyte nature of the corona is taken into account in a mean-field (the local osmotic balance) approximation.

By minimizing the free energy per chain in a micelle of given morphology i,

$$F^{(i)}(s) = F^{(i)}_{\text{core}}(s) + F^{(i)}_{\text{interface}}(s) + F^{(i)}_{\text{corona}}(s) \qquad (2)$$

we obtain the value of the core/corona interfacial area per chain s in the thermodynamically stable (or metastable) aggregate of morphology i and the corresponding free energy per chain $F^{(i)}$ as a function of the system parameters (degrees of polymerization N_A and N_B, volume fraction of condensed polymer in the core τ, bulk degree of ionization α_b and concentration of added salt Φ_{ion}).

The aggregates which have the minimal free energy, $F = \min\{F^{(i)}\}$, are thermodynamically stable. Aggregates of other morphologies correspond to the metastable states. The transition between morphologies i and $i \pm 1$ occurs as a thermodynamic first-order phase transition upon variation in any of the external parameters, e.g. temperature, salinity or pH.

3.1. Free Energy of the Core. The elastic free energy of an extended core block B yields

$$\frac{F^{(i)}_{\text{core}}(R)}{k_B T} = b_i \frac{R^2}{N_B} \qquad (3)$$

where

$$b_i = \begin{cases} \pi^2/8, & i = 1 \\ \pi^2/16, & i = 2 \\ 3\pi^2/80, & i = 3 \end{cases} \qquad (4)$$

The values of numerical coefficients in eq 4 reflect the nonuniform and nonequal extension of the core blocks in micelles of different morphologies. They were calculated in ref 28 for a dense micellar core with polymer volume fraction $\tau = 1$ but remain valid also for a condensed core with $\tau < 1$ (provided that the polymer density profile in the core is uniform).

We note that the free energy of nonelectrostatic interactions in the condensed core is determined only by the values of $v_B \simeq \tau$, w_B, and N_B and does not depend on the morphology or aggregation number of the micelle. We therefore omit this contribution from further consideration.

3.2. Free Energy of the Interface. The excess free energy of the core/corona interface per chain in aggregate of morphology i is given by

$$F^{(i)}_{\text{interface}}(R)/k_B T = \gamma s(R), \quad i = 1, 2, 3 \qquad (5)$$

where

$$s(R) = \frac{iN_B}{\tau R}, \quad i = 1, 2, 3 \qquad (6)$$

is the interfacial area per chain, as imposed by the condition of uniform polymer density $\cong -v_B/w_B = \tau$ in the condensed core of the micelle.[27] $k_B T\gamma$ is the surface free energy per unit area. When polymer volume fraction in the core $\tau \ll 1$, γ is related to τ by simple scaling relation[27] as $\gamma \cong \tau^2$. Below, however, we keep γ as an independent parameter to incorporate arbitrary values of $\tau \leq 1$ in the model.

3.3. Free Energy of Corona. In the strong segregation limit (corresponding to the narrow core/corona interface), the corona of a micelle is envisioned as a curved (in a spherical, $i = 3$, or cylindrical, $i = 2$, micelle) or as a planar (in a lamellar aggregate, $i = 1$) annealing polyelectrolyte brush.[29−31] To calculate the free energy of the polyelectrolyte brush, we employ the combination of the mean-field and the local electroneutrality approximations. The latter one assumes that the local excess (number) density of counterions inside the corona is approximately equal to the local (number) density of charged monomers. The details of the approach can be found in ref 21.

As long as the concentrations (or chemical potentials) of all the mobile ions in bulk solution are kept constant, the relevant free energy of the corona is the Gibbs free energy

$$F^{(i)}_{\text{corona}} = \frac{3k_B T}{2}\int_R^D \left(\frac{dr}{dn}\right) dr + \int_R^D f_{\text{int}}(c_p(r),\{c_j(r)\},\{c_{bj}\}) s(r)\, dr \qquad (7)$$

Here, the first term accounts for the elastic stretching of the extended coronal block whereas the second term accounts for the excluded volume interactions, the translational entropy of mobile ions, and the gain in the free energy due to corona ionization

$$f_{\text{int}}(c_p(r),\{c_j(r)\},\{c_{bj}\})/k_B T = v_A c_p^{\,2}(r) + \sum_j c_j(r)(\ln c_j(r) - 1) + \pi_b/k_B T - \sum_j c_j(r) \ln c_{bj} + c_p(r)[\alpha(r) \ln \alpha(r) + (1 - \alpha(r)) \ln(1 - \alpha(r)) + \alpha(r) \ln c_{bH^+} - \alpha(r) \ln K] \qquad (8)$$

where $\pi_b/k_B T = \Phi_{\text{ion}} = \sum_j c_{bj}$. Here $c_j(r)$ is the local concentration of ion of type j, and $c_p(r)$ and $\alpha(r)$ are the concentration of monomers and the degree of ionization in the corona at distance r from the center of the micelle, respectively. c_{bj} is the concentration of ions of type j in the bulk of the solution.

The local chain extension at distance r from the center of micelle, dr/dn, is related to local concentration of monomers $c_p(r)$ as

$$c_p(r) = \frac{dn}{s(r)\, dr} \qquad (9)$$

where

$$s(r) = s(R)\left(\frac{r}{R}\right)^{i-1}, \quad i = 1, 2, 3 \qquad (10)$$

By combining the condition of local ionization balance

$$\frac{\alpha(r)}{1 - \alpha(r)} = \frac{K}{c_{H^+}(r)} \qquad (11)$$

with the local electroneutrality condition

$$\sum_{j^-} c_{j^-}(r) + \alpha(r)c_p(r) = \sum_{j+} c_{j^+}(r) \tag{12}$$

and the Donnan rule

$$c_{j^-}(r)/c_{bj^-} = c_{bj^+}/c_{j^+}(r) \tag{13}$$

we represent the free energy of the corona (eq 7) as

$$F^{(i)}_{corona} = \int_R^D f\{c_p(r)\}s(r)\,dr \tag{14}$$

Here

$$f\{c_p(r)\}/k_BT = \frac{3}{2c_p(r)s^2(r)} + v_A{c_p}^2(r) - (\sqrt{1 + (\alpha(r)c_p(r)/\Phi_{ion})^2} - 1)\Phi_{ion} + c_p(r)\ln(1 - \alpha(r)) \tag{15}$$

is the density of corona free energy and $\alpha(r) = \alpha(c_p(r), \Phi_{ion})$ is determined by eqs 1, 13, and 11 as

$$\frac{\alpha(r)}{1-\alpha(r)}\frac{1-\alpha_b}{\alpha_b} = \sqrt{1 + (\alpha c_p(r)/\Phi_{ion})^2} - \alpha(r)c_p(r)/\Phi_{ion} \tag{16}$$

Thickness D of the corona is related to polymer density profile $c_p(r)$ and degree of polymerization of the coronal block N_A through normalization condition

$$\int_R^D c_p(r)s(r)\,dr = N_A \tag{17}$$

Polymer density profile $c_p(r)$ and radius of the corona D are found from minimization of the corona free energy, eq 14, under the constraint of eq 17 to give

$$\frac{\delta}{\delta c_p(r)} f\{c_p(r)\} = \lambda \tag{18}$$

$$\left(\frac{\delta}{\delta c_p(r)}\left[\frac{f\{c_p(r)\}}{c_p(r)}\right]\right)_{r=D} = 0 \tag{19}$$

Here $\lambda = \text{const}(r)$ is the exchange chemical potential which is constant throughout the corona. Equation 19 is equivalent to the condition of vanishing of the differential osmotic pressure at the edge of the corona, $r = D$. In the case of a planar brush ($i = 1$) polymer density c_p does not depend on distance r, and eq 19 is sufficient to find the equilibrium value of c_p and the corresponding values of thickness $H^{(1)}$ and free energy $F^{(1)}_{corona}$ of the planar corona.

Equations 7−18 allow us to calculate free energy of the corona $F^{(i)}_{corona}$ for any micelle morphology, $i = 1$, 2, and 3, and for arbitrary curvature of the core R as a function of the system parameters N_A, N_B, v_A, α_b, and Φ_{ion}.

Equations 15 and 16 can be expanded in powers of $\alpha(r)c_p(r)/\Phi_{ion}$, which is either large or small in the low salt and high salt asymptotic limits, respectively. As a result, one gets the following equations for the degree of ionization

$$\alpha(r) \cong \begin{cases} \sqrt{\frac{1}{2}\frac{\alpha_b}{1-\alpha_b}\frac{\Phi_{ion}}{(c_p(r))}} & \alpha c_p/\Phi_{ion} \gg 1 \\ \alpha_b\left(1 - \frac{\alpha_b c_p(r)}{\Phi_{ion}}(1-\alpha_b)\right) & \alpha c_p/\Phi_{ion} \ll 1 \end{cases} \tag{20}$$

and for the corresponding density of the corona free energy

$$\frac{f(c_p(r), \Phi_{ion})}{k_BT} \cong v_A{c_p}^2(r) + \frac{3}{2c_p(r)s^2(r)} + \begin{cases} -\alpha(r)c_p(r) + c_p(r)\ln(1-\alpha(r)) & \alpha c_p/\Phi_{ion} \gg 1 \\ \frac{{a_b}^2{c_p(r)}^2}{2\Phi_{ion}} + c_p(r)\ln(1-\alpha_b) & \alpha c_p/\Phi_{ion} \ll 1 \end{cases} \tag{21}$$

4. Starlike Spherical Micelles

In our previous publication,[21] we focused on the micelles of spherical morphology ($i = 3$) and considered thermodynamically stable and metastable states of a spherical micelle. The stable spherical micelle can be either starlike (referred to as S in ref 21) or a crew cut (referred to as CC1 in ref 21). The spherical micelle formed by a diblock with long insoluble block (referred to as CC2 in ref 21) is always metastable. (The equilibrium micelle morphology changes prior to onset of the crew cut CC2 regime).

As discussed in refs 20−22, the starlike micelles with size of the corona $D \gg R$ are formed by copolymers with sufficiently long block A

$$N_A \gg (N_B/\tau)^{5/7}\gamma^{2/7}{v_A}^{-3/7} \tag{22}$$

This condition holds for diblocks with an arbitrary degree of ionization α (including the case of a neutral amphiphile, $\alpha = 0$). In this range of molecular weights of the blocks, a starlike spherical micelle ($i = 3$) is the most favorable one. Micelles of other morphologies ($i = 1$ and $i = 2$) are metastable (thermodynamically less favorable than a spherical micelle). This is due to the geometry of the corona, minimizing the overlap and, therefore, the repulsive interaction between the coronal blocks. The thermodynamic and structural properties of a spherical starlike micelle with annealing polyelectrolyte corona were discussed in scaling terms in ref 21. Here we present a brief summary of the results and complement them with explicite calculation of relevant numerical factors.

Equilibrium parameters of a micelle in the starlike regime can be obtained by balancing the interfacial free energy $F_{interface}$ given by eq 5 and the corona free energy $F^{(3)}_{corona}$ calculated in Appendix 1. The contribution due to extension of the core block $F^{(3)}_{core}$ is negligible. In the low salt regime, the hydrophilic block in the starlike micelle is almost noncharged ($\alpha \ll \alpha_b$), and density of the corona free energy $f\{c_p(r)\}$ is given by eq 21 at $\alpha c_p \gg \Phi_{ion}$. In the high salt regime, the degree of ionization of the hydrophilic block $\alpha \approx \alpha_b$, and density of the corona free energy $f\{c_p(r)\}$ is given by eq 21 at $\alpha c_p \ll \Phi_{ion}$. By balancing $F^{(3)}_{corona}$ with $F_{interface}$, we obtain the equilibri-

um free energy per chain $F^{(3)}$ in a starlike micelle. In the low salt regime it is given by

$$F^{(3)}_{\text{lowsalt}}/k_BT \approx \frac{11 \times 3^{21/11}}{5^{16/11} \times 2^{4/11}} \frac{J_2^{5/11}}{J_1^{1/11}} \left(\frac{N_B}{\tau}\right)^{4/11} \gamma^{6/11} v_A^{2/11} N_A^{1/11} \quad (23)$$

whereas in the high salt regime

$$F^{(3)}_{\text{highsalt}}/k_BT \approx \frac{11 \times 3^{21/11}}{5^{16/11} \times 2^{4/11}} \frac{J_2^{5/11}}{J_1^{1/11}} \left(\frac{N_B}{\tau}\right)^{4/11} \gamma^{6/11} \left(v_A + \frac{\alpha^2}{2\Phi_{\text{ion}}}\right)^{2/11} N_A^{1/11} + N_A \ln(1 - \alpha_b) \quad (24)$$

The values of numerical prefactors J_1 and J_2 are calculated in Appendix 1, $J_1 \approx 0.325$ and $J_2 \approx 1.697$.

The total size of the micelle is dominated by corona thickness D. In both the low salt and high salt regimes

$$D \approx \frac{5^{3/11} \times 2^{9/11}}{3^{17/11} J_2^{3/11} J_1^{6/11}} \gamma^{3/11} v^{1/11} N_A^{6/11} \left(\frac{N_B}{\tau}\right)^{2/11} \quad (25)$$

with $v = v_A$ or $v = v_A + \alpha^2/2\Phi_{\text{ion}}$, respectively. Interfacial area per chain s, core radius R and aggregation number p are given respectively by

$$s = \frac{3^{21/11}}{5^{5/11} 2^{4/11}} \frac{J_2^{5/11}}{J_1^{1/11}} v^{2/11} \gamma^{-5/11} \tau^{-4/11} N_A^{1/11} N_B^{4/11} \quad (26)$$

$$R = \frac{3N_B}{\tau s} \simeq v^{-2/11} \gamma^{5/11} \tau^{-7/11} N_A^{-1/11} N_B^{7/11} \quad (27)$$

and

$$p = \frac{4\pi R^2}{s} \cong v^{-6/11} \gamma^{15/11} \tau^{-10/11} N_A^{-3/11} N_B^{10/11} \quad (28)$$

Note that due to the mean-field description of the corona, the exponents in eqs 25−28 are slightly different from the results of scaling model in ref 23.

At low salt concentrations a quasi-neutral spherical starlike micelle is thermodynamically favorable due to the gain in the free energy of the core/corona interface per chain. Here, the corona is weakly ionized, $\alpha \ll \alpha_b \leq 1$. Progressive increase in the salt concentration promotes ionization of the coronal chains, and at a certain value of salt concentration $\Phi_{\text{ion}} \cong \Phi^*_{\text{ion}}$, where

$$\Phi^*_{\text{ion}} \cong \alpha_b^{-7/2} (N_B/\tau)^2 \gamma^3 N_A^{-5} \quad (29)$$

the free energies per chain in a quasi-neutral large micelle (eq 23) and in a strongly charged small micelle (eq 24) become equal.[32] Equation 29 was obtained by expanding $\ln(1 - \alpha_b) \approx -\alpha_b$ in eq 24, and the numerical coefficient on the order of unity in eq 29 is omitted.

At $\Phi_{\text{ion}} \geq \Phi^*_{\text{ion}}$ a small charged micelle becomes more favorable. Although the area of core/corona interface per chain s increases, the strong ionization of the corona block provides the overall gain in the free energy per chain. As a result, the large quasi-neutral ($\alpha \ll \alpha_b$) starlike micelle decomposes spontaneously into smaller micelles with strongly charged corona, $\alpha \cong \alpha_b$. Aggregation number p drops down by the factor of $(1 + \alpha_b^2/2\Phi^*_{\text{ion}} v_A)^{6/11}$. The jump up in degree of ionization of the corona block α, that occurs at $\Phi_{\text{ion}} \cong \Phi^*_{\text{ion}}$, is accompanied by the jump up in corona thickness D, by the factor of $(1 + \alpha_b^2/2\Phi^*_{\text{ion}} v_A)^{1/5}$. Upon subsequent increase in the salt concentration aggregation number p in the charged starlike micelle progressively increases, while corona thickness D weakly decreases; see eq 25.

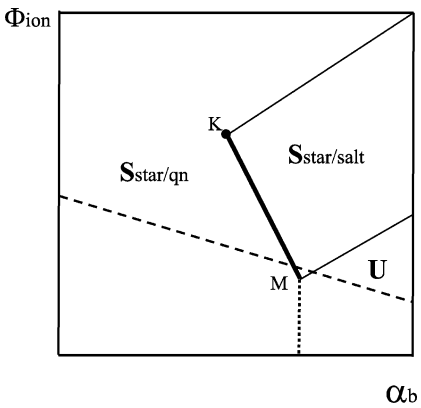

Figure 2. Diagram of states of diblock copolymer solution in α_b, Φ_{ion} coordinates for $N_A \gg (N_B/\tau)^{5/7}\gamma^{2/7}v_A^{-3/7}$, spherical starlike micelles. The bold line **K**−**M** indicates abrupt transition between large micelles with weakly ionized (quasi-neutral) coronae and small micelles with strongly ionized (salt-dominated) coronae. Positions of points **K** and **M** are specified as ($\alpha_b \simeq N_B^{4/11} N_A^{-10/11}$, $\Phi_{\text{ion}} \simeq N_B^{8/11} N_A^{-20/11}$) and ($\alpha_b \simeq N_B^{2/3} N_A^{-1}$, $\Phi_{\text{ion}} \simeq N_B^{-3/2} N_A^{-1/3}$).

Hence, both aggregation number p and corona thickness D vary discontinuously and nonmonotonically as a function of salt concentration Φ_{ion}. The former passes through a minimum, while the latter exhibits a maximum. The jumplike rearrangement of the spherical starlike micelle is expected in the range of relatively low ionic strength and the pH where $v_A \ll \alpha_b^2/2\Phi_{\text{ion}}$. In solutions with larger ionic strength, $v_A \gg \alpha_b^2/2\Phi_{\text{ion}}$, the micelle rearranges continuously. The phase diagram of diblock copolymer solution in α_b, Φ_{ion} coordinates (Figure 4a in ref 21) is reproduced in Figure 2.

5. Crew Cut Micelles

The crew cut micelle with thickness of the corona $H = D - R$ smaller than the core size R is formed by copolymer with shorter hydrophilic block A, $N_A \leq (N_B/\tau)^{5/7}\gamma^{2/7}v_A^{-3/7}$. In this range of molecular weights of the blocks, one finds a variety of aggregates of different morphologies. At high salt concentrations, where the annealing polyelectrolytes are virtually indistinguishable from the quenched ones, an increase in the solution salinity triggers the morphological transitions S−C−L.[22] As we demonstrate below, at low ionic strength in the solution the annealing nature of the coronal block leads to inversion of order of these transitions, and an increase in the solution salinity triggers L−C−S transformations in micelle morphology.

To give a unified description of the morphological transitions between the crew cut aggregates, we expand the corona free energy $F^{(i)}_{\text{corona}}$ with respect to small parameter $H/R \ll 1$ and retain only linear in curvature terms. The details of this calculation are collected in Appendix 2. In the limit of small curvature of the core, $H/R \ll 1$, the corona of crew cut aggregate of morphology

i is envisioned as a quasi-planar brush, and the free energy per chain (eq A2.22) is given by

$$F^{(i)}_{\text{corona}} \approx F^{(1)}_{\text{corona}} - \frac{3(i-1)}{2}\left(\frac{H^{(1)}}{N_A^{1/2}}\right)^2 \frac{H^{(1)}}{R} \qquad (30)$$

Here, $H^{(1)}$ and $F^{(1)}_{\text{corona}}$ are the thickness and the free energy (per chain) in a planar brush with the area $s(R)$ per chain. The specific expressions for thickness $H^{(1)}$ and free energy $F^{(1)}_{\text{corona}}$ depend on the range of the ionic strength and the pH. We start with the low salt regime where the annealing effects in the corona are important. We then briefly summarize the results for the high salt (salt dominance) regime where the aggregation behavior of the annealing and the quenched block polyelectrolytes is essentially equivalent.[22]

5.1. Low Salt Regime.

5.1.1. Quasi-Neutral Limit. In the quasi-neutral limit, the corona free energy is dominated by the nonelectrostatic excluded volume interactions, the second virial coefficient $v = v_A$. Here, the degree of corona ionization is small, $\alpha \ll v_A c_p$. By applying eq 30 we find that in the quasi-neutral limit corona free energy $F^{(i)}_{\text{corona}}$ in a crew cut micelle of morphology i is given by

$$F^{(i)}_{\text{corona}} \approx F^{(1)}_{\text{corona}}\left(1 - \frac{(i-1)}{3}\frac{H^{(1)}}{R}\right) \qquad (31)$$

Here,

$$F^{(1)}_{\text{corona}}/k_BT = \frac{3^{4/3}}{2} N_A v_A^{2/3} s^{-2/3}(R) \qquad (32)$$

and

$$H^{(1)} = H^{(1)}_0 = \frac{1}{3^{1/3}} N_A v_A^{1/3} s^{-1/3}(R) \qquad (33)$$

are the free energy and the thickness of a planar brush with area $s(R)$ per chain in the quasi-neutral limit, respectively (see Appendix 1). Index "0" indicates the neutral state of the micelle, $\alpha_b = 0$.

By using expansion 31, the free energy per chain in a crew cut micelle of morphology i can be represented as

$$F^{(i)}(s)/k_BT \approx F^{(1)}(s)/k_BT - \frac{(i-1)}{2i}\frac{N_A^2 v_A \tau}{N_B} + \gamma s + b_i \frac{i^2 N_B}{\tau^2 s^2}, \quad i = 1, 2, 3 \qquad (34)$$

where area per chain $s = s^{(i)}(R)$ is related to core radius R through eq 6. Here, the first term is the free energy of planar corona $F^{(1)}(s)$ is given by eq 32. The second (negative) term is the linear in curvature correction due to the cylindrical or spherical shape of the micelle. In the framework of the mean-field approximation, this term does not depend on core radius R but varies with micelle morphology i. (For a spherical micelle, $i = 3$, the decrease in the corona free energy due to core curvature is larger than for a cylindrical micelle, $i = 2$). The third term is the surface free energy of core/corona interface whereas the last term accounts for the elastic stretching of the core block. We note that, in the crew cut regime, the core contribution (the last term on rhs in eq 34) is still small with respect to the first term in the corona free energy. Therefore, the equilibrium radius of the micelle is determined predominantly by the balance of the first and the third terms in eq 34, whereas the forth term induces only small correction.

Minimization of the free energy $F^{(i)}$, eq 34, with respect to surface area per chain s gives

$$s = s_0 = 3^{1/5}\left(\frac{N_A}{\gamma}\right)^{3/5} v_A^{2/5} \qquad (35)$$

In the quasi-neutral limit, the free energy per chain in a micelle of morphology i (given with the accuracy of linear in curvature terms) yields

$$F^{(i)}/k_BT \approx \frac{5}{2} 3^{1/5} N_A^{3/5} v_A^{2/5} \gamma^{2/5} - \frac{(i-1)}{2i}\frac{N_A^2 v_A \tau}{N_B} + b_i \frac{i^2}{3^{2/5}}\frac{N_B}{\tau^2}\left(\frac{\gamma}{N_A v_A^{2/5}}\right)^{6/5} \quad i = 1, 2, 3 \qquad (36)$$

The transition between morphologies i and $i + 1$ is determined by the condition $F^{(i)} = F^{(i+1)}$ and can be triggered by, e.g., variations in temperature that affect v_A or/and γ. Equation 36 allows us to obtain the approximate expression for the binodal line corresponding to coexistence of micelles with morphology i and $i + 1$ ($i = 2, 1$)

$$v_{A,i\to i+1} \approx \frac{N_B^{10/9}}{N_A^{16/9}}\frac{\gamma^{2/3}}{\tau^{5/3}}\left[\frac{2i(i+1)}{3^{2/5}}(b_{i+1}(i+1)^2 - b_i i^2)\right]^{5/9} \qquad (37)$$

We emphasize that the values of exponents in eq 37 are obtained in the framework of a mean-field model of polymer solution and are slightly different from the scaling results.[33]

5.1.2. Annealing Osmotic Limit. At relatively small salt concentration in the solution when the degree of corona ionization $v_A c_p \ll \alpha \ll \alpha_b$, a crew cut micelle is found in the osmotic annealing limit. Here, degree of ionization $\alpha(r)$ and density of the free energy $f\{c_p(r)\}$ are given by the corresponding eqs 20 and 21 at $\alpha c_p/\Phi_{\text{ion}} \gg 1$. By using eq 19 we first calculate polymer density c_p, free energy $F^{(1)}_{\text{corona}} = N_A f\{c_p\}/c_p$, and thickness $H^{(1)} = N_A/sc_p$ for the planar brush, and then apply eq 30. We find

$$F^{(i)}_{\text{corona}} \approx F^{(1)}_{\text{corona}}\left(1 + \frac{(i-1)}{3}\frac{H^{(1)}}{R}\right) \qquad (38)$$

Here,

$$F^{(1)}_{\text{corona}}/k_BT = -\frac{(3\sqrt{2})^{2/3}}{4} N_A s^{2/3}(R)\left(\frac{\alpha_b \Phi_{\text{ion}}}{1-\alpha_b}\right)^{2/3} \qquad (39)$$

and

$$H^{(1)} = \frac{1}{(3\sqrt{2})^{2/3}} N_A s^{1/3}(R)\left(\frac{\alpha_b \Phi_{\text{ion}}}{1-\alpha_b}\right)^{1/3} \qquad (40)$$

are the corona free energy and the corona thickness in the planar annealing osmotic brush with area $s(R)$ per chain.

The free energy per chain in a crew cut micelle of morphology i in the osmotic annealing limit yields

$$F^{(i)}(s)/k_BT \approx F^{(1)}(s)/k_BT - \frac{(i-1)}{12i}\frac{N_A{}^2 s^2 \tau}{N_B}\left(\frac{\alpha_b\Phi_{ion}}{1-\alpha_b}\right) + \gamma s + b_i\frac{i^2 N_B}{\tau^2 s^2} \quad i = 1, 2, 3 \quad (41)$$

where area per chain $s = s^{(i)}(R)$ is related to core radius R through eq 6. Balance of the first and the third terms in eq 41 gives the equilibrium value of area per chain s,

$$s = \frac{1}{12}\left(\frac{N_A}{\gamma}\right)^3\left(\frac{\alpha_b\Phi_{ion}}{1-\alpha_b}\right)^2 \quad (42)$$

Note that in the osmotic annealing limit, interfacial area per chain s increases upon an increase in salt concentration Φ_{ion}. The core radius

$$R = \frac{iN_B}{\tau s} \simeq \left(\frac{\gamma}{N_A}\right)^3\left(\frac{N_B}{\tau}\right)\left(\frac{\alpha_b\Phi_{ion}}{1-\alpha_b}\right)^{-2} \quad (43)$$

and the aggregation number (in spherical micelles)

$$p = \frac{4\pi R^2}{s} \simeq \left(\frac{\gamma}{N_A}\right)^9\left(\frac{N_B}{\tau}\right)^2\left(\frac{\alpha_b\Phi_{ion}}{1-\alpha_b}\right)^{-6} \quad i = 3 \quad (44)$$

decrease, whereas the corona thickness

$$H^{(i)} \cong H^{(1)} \simeq \frac{N_A{}^2}{\gamma}\left(\frac{\alpha_b\Phi_{ion}}{1-\alpha_b}\right) \quad (45)$$

increases as a function of Φ_{ion}.

The corresponding free energy per chain in aggregate of morphology i is given (with accuracy of linear in core curvature terms) by

$$F^{(i)}/k_BT \approx -\frac{1}{24}\frac{N_A{}^3}{\gamma^2}\left(\frac{\alpha_b\Phi_{ion}}{1-\alpha_b}\right)^2 - \frac{i-1}{i}\left(\frac{1}{12}\right)^3\frac{N_A{}^8\tau}{N_B\gamma^6}\left(\frac{\alpha_b\Phi_{ion}}{1-\alpha_b}\right)^5 + i^2 b_i (12)^2\frac{N_B\gamma^6}{\tau^2 N_A{}^6}\left(\frac{\alpha_b\Phi_{ion}}{1-\alpha_b}\right)^{-4} \quad (46)$$

The condition $F^{(i)} = F^{(i+1)}$ determines the transition between the crew cut micelles of morphology i and $i+1$, $i = 1, 2$. The binodal line is given by

$$\left(\frac{\alpha_b\Phi_{ion}}{1-\alpha_b}\right)_{i\to i+1} = 3^{5/9}2^{10/9}\frac{N_B{}^{2/9}\gamma^{4/3}}{\tau^{1/3}N_A{}^{14/9}}[i(i+1)[(i+1)^2 b_{i+1} - i^2 b_i]]^{1/9} \quad (47)$$

It follows from eq 47 that an increase in the solution salinity (an increase in Φ_{ion}) as well as an increase in the pH can trigger the morphological transitions between crew cut micelles in the osmotic annealing regime. By substituting the values of numerical coefficients b_i from eq 4 in eq 47, we find that binodal line for L−C transition ($i = 1$) is located at smaller value of Φ_{ion} than binodal line for C−S transition ($i = 2$). Therefore, an increase in the ionic strength in solution leads to L → C → S transformations in a crew cut micelle with annealing osmotic corona.

As we discuss below, due to weak ionization of the coronal chains in the annealing osmotic regime, the effect of the excluded volume interactions is nonnegligible and siginficantly modifies the shape of the binodals in comparison to those given by eq 47. To take into account the contribution of the excluded volume interactions to the free energy of the corona in the annealing osmotic regime we can expand the logarithmical term in eq 21 making use of the fact, that $\alpha \ll \alpha_b \leq 1$.

By applying eq 19 we obtain the polymer density profile c_p

$$c_p = \left(-\frac{1}{2v_A}\sqrt{\frac{\alpha_b\Phi_{ion}}{2(1-\alpha_b)}} + \sqrt{\frac{\alpha_b\Phi_{ion}}{8v_A{}^2(1-\alpha_b)} + \frac{3}{v_A s^2}}\right)^{2/3} \quad (48)$$

Then, the free energy per chain in the planar corona, $F^{(1)}_{corona} = f(c_p)sH^{(1)} = f(c_p)N_A/c_p$, and the corona thickness, $H^{(1)} = N_A/sc_p$, can be presented as

$$F^{(1)}_{corona}/k_BT = \gamma s_0\frac{3}{2u^{1/3}}\frac{\sqrt{1+\frac{u}{t^2}}-3}{\left(\sqrt{1+\frac{u}{t^2}}-1\right)^{1/3}} \quad (49)$$

and

$$H^{(1)} = H_0^{(1)}\frac{u^{1/3}}{\left(\sqrt{1+\frac{u}{t^2}}-1\right)^{2/3}} \quad (50)$$

where $H_0{}^{(1)}$ is the corona thickness in the quasi-neutral limit given by eq 33. We introduce at this stage the reduced variables

$$t = \frac{s}{s_0} = \frac{s}{3^{1/5}v_A{}^{2/5}}\left(\frac{\gamma}{N_A}\right)^{3/5} \quad (51)$$

and

$$u = \frac{(1-\alpha_b)}{\Phi_{ion}\alpha_b}\frac{24v_A}{s_0{}^2} = \frac{(1-\alpha_b)}{\Phi_{ion}\alpha_b}\frac{24v_A{}^{1/5}}{3^{2/5}}\left(\frac{\gamma}{N_A}\right)^{6/5} \quad (52)$$

where s_0 is the interfacial area per chain in the quasi-neutral limit, eq 35.

Following the same route as before (i.e., by using eq 30), we present the coronal free energy in the crew cut micelle of morphology i as

$$F^{(i)}_{corona} \approx F^{(1)}_{corona}\left\{1 - (i-1)\frac{H^{(1)}}{R}\frac{u}{3t^2}\times \frac{1}{\left(\sqrt{1+\frac{u}{t^2}}-1\right)\left(\sqrt{1+\frac{u}{t^2}}-3\right)}\right\} \quad (53)$$

By balancing the dominant contribution in the coronal free energy, $F^{(i)}_{corona} \approx F^{(1)}_{corona}$ (eq 49), with surface free energy, $F_{interface} = \gamma s k_B T = \gamma s_0 t k_B T$, we find the equilibrium value of area s per chain or, equivalently, the

relation between t and u,

$$\frac{u^{2/3}}{t^3\left(\sqrt{1+\frac{u}{t^2}}-1\right)^{4/3}}=1 \qquad (54)$$

The equation for binodals is obtained along the same lines as before. One obtains after some algebra

$$\frac{N_B{}^2\gamma^{6/5}}{\tau^3 N_A{}^{16/5} v_A{}^{9/5} t(u)^{9/2}}\left[\frac{2}{3^{2/5}} i(i+1)[(i+1)^2 b_{i+1} - i^2 b_i]\right] = 1 \qquad (55)$$

where $t(u)$ is given by eq 54.

When $u \to \infty$ (or, equivalently, $\alpha_b \to 0$), $t(u) \to 1$, and eq 55 reduces to eq 37 for binodals in the quasi-neutral limit. In the annealing osmotic limit $u \to 0$, and $t(u) \to 16/u^2$. Here, eq 55 reduces to eq 47. For intermediate values of $0 < u < \infty$, eq 55 determines the binodals with the account of both, the electrostatic and nonelectrostatic interactions in the corona of micelle.

5.2. High Salt Regime. In the high salt (or the so-called salt dominance) regime $\alpha c_p/\Phi_{ion} \ll 1$, $\alpha \approx \alpha_b = \text{const}(\Phi_{ion})$, and the coronal free energy is governed by the screened electrostatic interactions that give rise to the renormalized (effective) virial coefficient $v = v_A + \alpha_b{}^2/2\Phi_{ion}$. As discussed in ref 22, at constant $\alpha = \alpha_b$, an increase in the solution salinity (an increase in Φ_{ion}) leads to the decrease in the effective virial coefficient $v = v_A + \alpha_b{}^2/2\Phi_{ion}$ and triggers the morphological transitions between crew cut micelles.

By applying eq 30, we find that in the salt dominance regime corona free energy $F^{(i)}_{corona}$ in a crew cut micelle of morphology i is given by

$$F^{(i)}_{corona}/k_BT \approx [F^{(1)}_{corona}/k_BT - N_A \ln(1-\alpha_b)]\left(1+\frac{(1-i)}{3}\frac{H^{(1)}}{R}\right) + N_A \ln(1-\alpha_b) \qquad (56)$$

Here

$$F^{(1)}_{corona}/k_BT = \frac{3^{4/3}}{2} N_A \left(v_A + \frac{\alpha_b{}^2}{2\Phi_{ion}}\right)^{2/3} s^{-2/3}(R) + N_A \ln(1-\alpha_b) \qquad (57)$$

and

$$H^{(1)} = \frac{1}{3^{1/3}} N_A \left(v_A + \frac{\alpha_b{}^2}{2\Phi_{ion}}\right)^{1/3} s^{-1/3}(R) \qquad (58)$$

are the corona free energy and the corona thickness of a planar brush with area $s(R)$ per chain in the salt dominance regime (see Appendix 1).

The free energy per chain in crew cut micelle of morphology i yields

$$F^{(i)}/k_BT \approx \frac{5}{2}3^{1/5} N_A{}^{3/5} v^{2/5}\gamma^{2/5} - \frac{(i-1)}{2i}\frac{N_A{}^2 v\tau}{N_B} + b_i \frac{i^2}{3^{2/5}}\frac{N_B}{\tau^2}\left(\frac{\gamma}{N_A v^{2/5}}\right)^{6/5} + N_A \ln(1-\alpha_b), \quad i = 1, 2, 3 \qquad (59)$$

where $v = v_A + \alpha_b{}^2/2\Phi_{ion}$. The transitions between morphologies i and $i+1$ are determined by the condition $F^{(i)} = F^{(i+1)}$. Equation 59 allows us to obtain an expression for the binodal line corresponding to coexistence of micelles with morphology $i+1$ and i ($i = 2, 1$),

$$v_{i\to i+1} = v_A + \alpha_b{}^2/2\Phi_{ion}^{(i\to i+1)} \approx \frac{N_B{}^{10/9}}{N_A{}^{16/9}}\frac{\gamma^{2/3}}{\tau^{5/3}}\left[\frac{2i(i+1)}{3^{2/5}}(b_{i+1}(i+1)^2 - b_i i^2)\right]^{5/9} \qquad (60)$$

In the salt dominance regime, an increase in solution salinity leads to S → C → L morphological transitions in crew cut micelles. Equation 60 indicates that binodals for micelles with annealing polyelectrolyte blocks coincide with those for quenched ones, ref 22, at $\alpha = \alpha_b$.

We now summarize our findings by constructing the scaling type phase diagrams for the solution of diblock copolymer with an annealing polyelectrolyte block.

6. Phase Diagrams of Diblock Copolymer Solution

The complexity of the phase diagram of diblock copolymer solution is governed by relative degrees of polymerization of the blocks N_A and N_B. The phase diagram can contain different number of regions, each region representing the specific morphology of the micelle. In each of the regions the micelles are found when solution concentration exceeds the *cmc*. The values of *cmc* for spherical starlike and crew cut micelles were analyzed in ref 21. Because the characteristics of the crew cut aggregates of all the morphologies $i = 1, 2, 3$, obey the same scaling laws, the expression for *cmc* for a spherical crew cut micelle will be valid (with accuracy of the numerical coefficients) for a crew cut cylindrical and a lamellar aggregate as well. We therefore do not consider the *cmc* here, see ref 21 for detail.

6.1. Diagrams of State in Φ_{ion}, α_b Coordinates. Below we present a series of the scaling diagrams in the $\log(\Phi_{ion})$, $\log(\alpha_b)$ coordinates corresponding to different chemical compositions of block copolymer molecule, i.e., different degrees of polymerization of the ionic and hydrophobic blocks (Figures 2−5). We emphasize that these diagrams are schematic and are designed to demonstrate how different regions evolve upon variation in the molecular weight of hydrophilic block A. The scaling dependences for equilibrium parameters of micelles in different regimes are collected in Table 1, where $v = v_A + \alpha_b{}^2/2\Phi_{ion}$.

Bold solid lines in the diagrams indicate the first-order phase transitions, expressions for the binodals are given by eqs 47 and 60. Thin solid lines correspond to smooth crossover between the regimes. The scaling expressions for these boundaries can be derived by equating the micelle characteristics in Table 1 in the two neighboring regions.

The dashed line, $\log(\Phi_{ion}) \approx \log(K) - \log(\alpha_b)$, corresponds to the minimal values of Φ_{ion} that could be attained at given $\alpha_b = \alpha_b(\text{pH})$. Evidently, total ion concentration Φ_{ion} exceeds $10^{-\text{pH}}$ for pH < 7, or $10^{\text{pH}-14}$ for pH > 7. For an acidic monomer with $pK = -\log(K) < 7$, and $\alpha_b < 1$, the minimal value of $\Phi_{ion} \approx 10^{-\text{pH}} = 10^{-pK}(1-\alpha_b)/\alpha_b \approx 10^{-pK}/\alpha_b$.

The dotted line delineates the region U where block copolymer remains a unimer and does not associate into micelles. As this dotted line is approached from the left, the *cmc* rapidly increases. To the right from the dotted line, no micelles are found at any polymer concentration

Table 1

	α	R_{core}	H_{corona}	S
$S_{star/qn}$	$(\alpha_b\Phi_{ion}/(1-\alpha_b))^{1/2}N_A^{5/11}\,\upsilon_A^{9/22}\gamma^{-3/11}(N_B/\tau)^{-2/11}$	$(N_B/\tau)^{7/11}N_A^{-1/11}\,\upsilon_A^{-2/11}\gamma^{5/11}$	$N_A^{6/11}\,\upsilon_A^{1/11}\gamma^{3/11}(N_B/\tau)^{2/11}$	$(N_B/\tau)^{4/11}N_A^{1/11}\gamma^{-5/11}\upsilon_A^{2/11}$
$S_{star/salt}$	α_b	$(N_B/\tau)^{7/11}N_A^{-1/11}\upsilon^{-2/11}\gamma^{5/11}$	$N_A^{6/11}\upsilon^{1/11}\gamma^{3/11}(N_B/\tau)^{2/11}$	$(N_B/\tau)^{4/11}N_A^{1/11}\gamma^{-5/11}\upsilon^{2/11}$
$S,C,L_{cc/qn}$	$(\alpha_b\Phi_{ion}/(1-\alpha_b))^{1/2}N_A^{1/5}\,\upsilon_A^{3/10}\gamma^{-1/5}$	$(N_B/\tau)N_A^{-3/5}\,\upsilon_A^{-2/5}\gamma^{3/5}$	$N_A^{4/5}\,\upsilon_A^{1/5}\gamma^{1/5}$	$N_A^{3/5}\,\upsilon_A^{3/5}\gamma^{-3/5}$
$S,C,L_{cc/osm}$	$(\alpha_b\Phi_{ion}/(1-\alpha_b))^2N_A^2\gamma^{-2}$	$(N_B/\tau)N_A^{-3}\gamma^3(\alpha_b\Phi_{ion}/(1-\alpha_b))^{-2}$	$N_A^2\gamma^{-1}(\alpha_b\Phi_{ion}/(1-\alpha_b))$	$N_A^3\gamma^{-3}(\alpha_b\Phi_{ion}/(1-\alpha_b))^2$
$S,C,L_{cc/salt}$	α_b	$(N_B/\tau)N_A^{-3/5}\upsilon^{-2/5}\gamma^{3/5}$	$N_A^{4/5}\upsilon^{1/5}\gamma^{1/5}$	$N_A^{3/5}\upsilon^{2/5}\gamma^{-3/5}$

in the dilute solution. We remark, that in the case of sufficiently long B block/ short A block region U disappears from the diagram, i.e., for any (Φ_{ion}, α_b) a finite *cmc* exists above which the aggregates are formed in the solution.

We now briefly summarize the general features of the diagrams.

6.1.1. $N_A \gg (N_B/\tau)^{5/7}\gamma^{2/7}\upsilon_A^{-3/7}$**.** Diblock copolymer with asymmetric composition, $N_A \gg (N_B/\tau)^{5/7}\gamma^{2/7}\upsilon_A^{-3/7}$, forms only spherical starlike micelles in the whole range of pH and salt concentration Φ_{ion} (Figure 2). The diagram contains the following regions:

$S_{star/qn}$ corresponds to spherical starlike micelles with the corona dominated by the nonelectrostatic (excluded volume) interactions. Here, the coronal chains are weakly ionized.

$S_{star/salt}$ corresponds to spherical starlike micelles with strongly charged corona, $\alpha \cong \alpha_b$ (maximal degree of ionization at given pH in the bulk solution).

Region U corresponds to the range of parameters where the Coulomb repulsion prevents copolymer chains from aggregation at any concentration of the polymer in solution.

The bold line **K**−**M** separating $S_{star/qn}$ and $S_{star/salt}$ regions is given by eq 29 and corresponds to abrupt transformation of large quasi-neutral micelles into smaller charged micelles with strongly ionized corona, $\alpha \approx \alpha_b$. This transition can be induced either by variations in the ionic strength of the solution (Φ_{ion}) or by variations in the pH (which determines the value of α_b). The positions of points **K** and **M** are specified in the figure caption.

6.1.2. $C_1N_B^{5/8}\gamma^{3/8}\tau^{-15/16}\upsilon_A^{-9/16} \ll N_A \ll (N_B/\tau)^{5/7}\gamma^{2/7}\upsilon_A^{-3/7}$**.** In this interval of molecular weights copolymer with a neutral hydrophilic block associates into crew cut spherical micelles (Figure 3). The value of $C_1 = [21\pi^2/(2 \times 3^{2/5})]^{5/16} \approx 1.82$ corresponds to the binodal line for the S−C transition given by eq 37 at $i = 2$. In addition to already discussed $S_{star/salt}$ regime, the diagram contains the following regions.

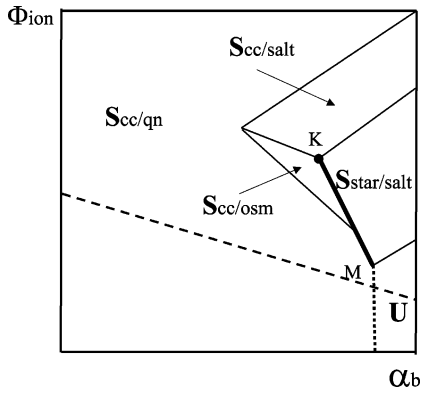

Figure 3. Diagram of states of diblock copolymer solution in α_b, Φ_{ion} coordinates for $C_1N_B^{5/8}\gamma^{3/8}\tau^{-15/16}\upsilon_A^{-9/16} \ll N_A \ll (N_B/\tau)^{5/7}\gamma^{2/7}\upsilon_A^{-3/7}$, spherical crew cut and starlike micelles. Positions of points **K** and **M** are specified as ($\alpha_b \simeq N_B^{2/3}N_A^{-4/3}$, $\Phi_{ion} \simeq N_B^{-1/3}N_A^{-1/3}$) and ($\alpha_b \simeq N_B^{2/3}N_A^{-1}$, $\Phi_{ion} \simeq N_B^{-3/2}N_A^{-1/3}$).

$S_{cc/qn}$ corresponds to the quasi-neutral regime of crew cut spherical micelles with $H \ll R$. Here, the structure of corona is governed by the excluded volume monomer−monomer interactions.

At sufficiently large α_b an increase in the salt concentration promotes corona ionization, and spherical crew cut micelles pass into the osmotic annealing regime, region $S_{cc/osm}$. In this regime, the degree of ionization of corona block A increases as a function of salt concentration (see Table 1). As a result, the Coulomb repulsion gets stronger and aggregation number p and core radius R decrease.

Eventually the degree of ionization of corona block A reaches α_b, and the micelle passes in the $S_{cc/salt}$ regime. Further evolution of the micelle upon an increase in the salt concentration is governed by the screened Coulomb repulsion between the coronal blocks. It occurs similarly to that for a micelle with a quenched polyelectrolyte block:[20,22] aggregation number p and core radius R increase, while the corona thickness H decreases as a function of salt concentration.

Depending on the value of α_b there are two different scenarios for evolution of the osmotic crew cut micelles upon an increase in salt concentration. In the range of $(\gamma\upsilon_A/N_A)^{2/5} \ll \alpha_b \ll \gamma^{2/3}(N_B/\tau)^{2/3}N_A^{-4/3}$ the micelle reaches the degree of ionization α_b preserving its crew cut shape. Then it continuously passes from $S_{cc/osm}$ into the $S_{cc/salt}$ regime. When, however, $\gamma^{2/3}(N_B/\tau)^{2/3}N_A^{-4/3} \ll \alpha_b \ll \gamma(N_B/\tau)^{2/3}N_A^{-1}$, the osmotic (as well as the quasi-neutral) crew cut micelle abruptly dissociates into charged starlike micelles. This transformation is accompanied by a jump in the degree of corona ionization up to α_b, and constitutes the first-order phase transition $S_{cc/osm} \rightarrow S_{star/salt}$ (or $S_{cc/qn} \rightarrow S_{star/salt}$). The transition line **K**−**M** is determined by eq 29, the positions of points **M** and **K** are specified in figure legend. Similarly to the case of starlike micelles, the free energy per chain in $S_{cc/osm}$ or $S_{cc/qn}$ regimes is much smaller than the absolute value of each of the two contributions to the free energy per chain in $S_{star/salt}$ regime (eq 24). Therefore, the transition occurs at salt concentration $\Phi_{ion} \approx \Phi_{ion}^*$. Here, the degree of corona ionization α jumps up to α_b, while the aggregation number p drops down. Upon further increase in the salt concentration the aggregation number p increases at virtually constant value of $\alpha \approx \alpha_b$ and the starlike micelle is continuously transformed back to the crew cut micelle (by passing into $S_{cc/salt}$ regime).

6.1.3. $C_2N_B^{5/8}\gamma^{3/8}\tau^{-15/16}\upsilon_A^{-9/16} \ll N_A \ll C_1N_B^{5/8}\gamma^{3/8}\tau^{-15/16}\upsilon_A^{-9/16}$**.** In this interval of molecular weights of the blocks, the diblock copolymer with a neutral hydrophilic block associates into cylindrical micelles. The value of $C_2 = [\pi^2/(2 \times 3^{2/5})]^{5/16} \approx 1.43$ corresponds to the binodal line for the C−L transition given by eq 37 at $i = 1$. The corresponding phase diagram is presented in Figure 4. The following additional regions are delineated.

$C_{cc/qn}$ is the regime of quasi-neutral crew cut cylindrical micelle. Here, the corona is almost neutral and its

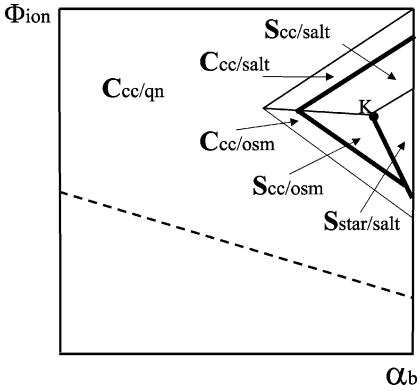

Figure 4. Diagram of states of diblock copolymer solution in α_b, Φ_{ion} coordinates for $C_2N_B^{5/8}\gamma^{3/8}\tau^{-15/16}\upsilon_A^{-9/16} \ll N_A \ll C_1N_B^{5/8}\gamma^{3/8}\tau^{-15/16}\upsilon_A^{-9/16}$, spherical starlike, spherical and cylindrical crew cut micelles. The coordinates of point **K** are the same as in Figure 3.

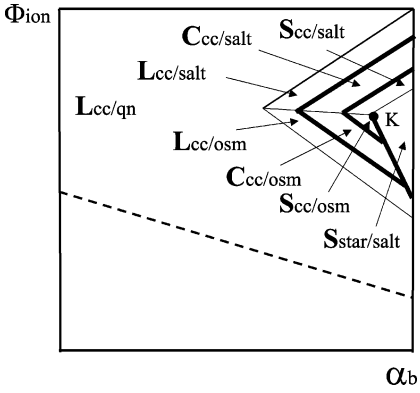

Figure 5. Diagram of states of diblock copolymer solution in α_b, Φ_{ion} coordinates for $N_A \ll C_2N_B^{5/8}\gamma^{3/8}\tau^{-15/16}\upsilon_A^{-9/16}$, spherical starlike, spherical, cylindrical, and lamellar crew cut aggregates. The coordinates of point **K** are the same as in Figure 3.

structure is governed by the excluded volume monomer−monomer interactions, $\upsilon = \upsilon_A$.

$C_{cc/osm}$ is the regime of annealing osmotic crew cut cylindrical micelle. Here, the osmotic pressure of mobile ions swells the quasi-planar corona, and aggregation number per unit length of the cylinder $\sim R/s$ decreases as a function of Φ_{ion}.

$C_{cc/salt}$ is the regime of crew cut cylindrical micelle with charged corona, $\alpha = \alpha_b$, dominated by screened electrostatic interactions between monomers, $\upsilon = \upsilon_A + \alpha_b^2/2\Phi_{ion}$.

All other regimes are described above. Note that for considered block copolymer compositions, the regime of unimers U disappears. Ionizable block A is now relatively short, and the electrostatic repulsion even between strongly charged corona blocks ($\alpha_b \approx 1$) cannot prevent association of polymeric amphiphiles in micelles at solution concentrations above *cmc*.

6.1.4. $N_A \ll C_2N_B^{5/8}\gamma^{3/8}\tau^{-15/16}\upsilon_A^{-9/16}$. Copolymer with this composition gives rise to the most sophisticated phase diagram, Figure 5.

Block copolymers with short neutral or weakly charged hydrophilic blocks give rise to crew cut lamellar aggregates with corona thickness $H \ll R$. The quasi-neutral regime $L_{cc/qn}$ occupies larger part of the diagram. The lamellar aggregates are quasi-neutral at low salt concentration and relatively small α_b and also behave as quasi-neutral ones at sufficiently high salt concentration and large α_b.

In the intermediate range of salt concentration and at sufficiently large $\alpha_b > N_A^{-2/5}$, a variety of morphologies and multiple morphological transitions are expected. We find here the regimes of lamellar osmotic annealing aggregates, $L_{cc/osm}$, cylindrical osmotic annealing micelles, $C_{cc/osm}$, spherical osmotic annealing micelles, $S_{cc/osm}$, as well as the regimes of strongly charged micelles, $L_{cc/salt}$, $C_{cc/salt}$, and $S_{cc/salt}$. The scaling dependences for equilibrium characteristics of the crew cut micelles of all the different morphologies coincide and are collected in Table 1. Depending on the value of α_b (controlled by the pH in the solution) an increase in ionic strength triggers the transitions L → C → L or L → C → S → C → L. In both cases, lamellar aggregates are found in the quasi-neutral regime in both, the low and high salt limits. Initial increase in Φ_{ion} leads to progressive ionization of corona blocks (transition $L_{cc/qn} \rightarrow L_{cc/osm}$) followed by the reversed morphological transitions $L_{cc/osm} \rightarrow C_{cc/osm} \rightarrow S_{cc/osm}$. The binodal lines for these transitions are given by eq 47. The degree of ionization α, area per chain s and corona thickness D in any two coexisting morphologies (e.g., $L_{cc/osm}$ and $C_{cc/osm}$ or $C_{cc/osm}$ and $S_{cc/osm}$) remain almost the same. Radius of the core R, however, drops according to eq 6. Further increase in Φ_{ion} leads to the rearrangement of spherical micelle first without morphology change, $S_{cc/osm} \rightarrow S_{cc/salt}$. When $\alpha_b < N_B^{2/3}/N_A^{4/3}$, this transformation is gradual. When $\alpha_b > N_B^{2/3}/N_A^{4/3}$, the crew cut osmotic annealing micelle first abruptly dissociates into smaller charged micelles (transition $S_{cc/osm} \rightarrow S_{star/salt}$) and then gradually passes from $S_{star/salt}$ to $S_{cc/salt}$ regime upon an increase in Φ_{ion}. The binodal line for the $S_{cc/osm} - S_{star/salt}$ transition is given by eq 29. At larger values of Φ_{ion}, the direct morphological transitions $S_{cc/salt} \rightarrow C_{cc/salt} \rightarrow L_{cc/salt}$ take place. The binodal lines are given by eq 60. Further increase in Φ_{ion} leads to progressive screening of the electrostatic interactions, and the lamellar aggregate finally approaches its quasi-neutral state, $L_{cc/qn}$. During this route, all characteristics of the micelles demonstrate nonmonotonic behavior as a function of salt concentration Φ_{ion}.

6.2. Diagrams of State in N_B, Φ_{ion} Coordinates. The scaling diagrams of previous subsection provide a systematic picture of micelle evolution caused by variations in the pH and the solution salinity. Each of the diagrams is obtained for diblock copolymer with a fixed chemical composition (fixed values of N_A and N_B). We now focus on the diagrams in the N_B, Φ_{ion} coordinates. Here, the pH in the solution (or equivalently α_b) is fixed whereas the diblock copolymer composition (degree of polymerization of solvophobic block B) is varied.

Figures 6 and 7 demonstrate the diagrams of diblock copolymer solution in the N_B, Φ_{ion} coordinates for two different values of $\alpha_b = 0.5$ and $\alpha_b = 0.1$, respectively. Values of other parameters are: $\gamma = 1$, $\upsilon = 0.4$, $\tau = 1$ and $N_A = 50$. The diagrams contain the regions of spherical (S), cylindrical (C), and lamellar (L) morphologies. The binodals, separating micelles of different morphologies demonstrate the nonmonotonic behavior as a function of salt concentration Φ_{ion}. The increasing branches of the binodals (low salt) are determined by eq 55, the decreasing branches (high salt) are plotted according to eq 60. The dotted lines in Figure 6a correspond to asymptotic expressions for the binodals, eqs 37 and 47. The dashed lines in Figure 6b correspond to the binodals for a noncharged copolymer, eq 37.

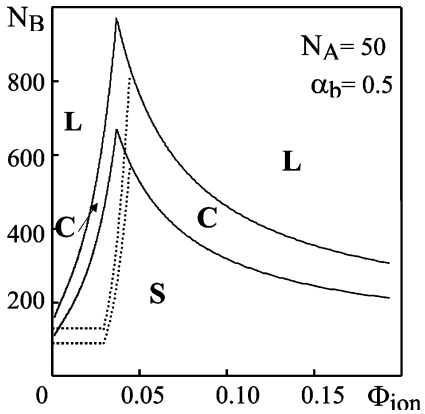

Figure 6. Diagram of states of diblock copolymer solution in N_B, Φ_{ion} coordinates for $\alpha_b = 0.5$ The values of other parameters are: $\gamma = 1$, $\tau = 1$, $\upsilon = 0.4$, and $N_A = 50$.

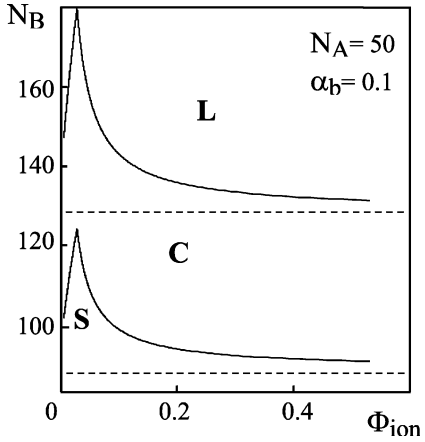

Figure 7. Diagram of states of diblock copolymer solution in N_B, Φ_{ion} coordinates for $\alpha_b = 0.1$. The values of other parameters are the same as in Figure 6.

The diagrams indicate that for sufficiently high pH (strongly charged copolymer, $\alpha_b = 0.5$), a variety of transition scenarios are possible. Depending on the value of N_B, the micelle transformations L−C−L, L−C−S−C−L, C−S are expected upon an increase in the ionic strength in the solution (the increase in Φ_{ion}). The asymptotes for the binodals (dotted lines) correctly reproduce the general trends in the binodal behavior. However, the numerical values of N_B corresponding to full and asymptotic expressions for binodals can deviate significantly. We note that the sharp maximum corresponding to the crossover of binodals would be smoothed if full solutions of eqs 15−19 for polymer density profile $c_p(r)$ and density of the free energy $f\{c_p(r)\}$ were used to derive the binodals.

A decrease in the degree of ionization α_b leads to reduction in the number of possible transitions. Figure 7 indicates that for $\alpha_b = 0.1$ only L−C−L and C−S−C transitions are expected. For certain values of N_B (around $N_B = 125$ in Figure 7) the micelle can even retain its cylindrical morphology at any ionic strength. A decrease in α_b causes the corresponding decrease of the binodal maximum and shifts this maximum to lower values of Φ_{ion}. When $\alpha_b \to 0$, the binodals approach the dashed lines corresponding to the binodals for a neutral diblock copolymer.

7. Discussion and Conclusions

We have developed a theory to describe association of diblock copolymer amphiphile with weakly dissociating (pH-sensitive) polyelectrolyte block in dilute solution. In this work we focus on the analysis of morphological transitions for micelles with weakly ionizable corona. The "reversed" sequence of L−C−S transitions takes place at relatively small ionic strength in the solution and can be triggered by variations in the solution salinity or the pH. At large ionic strength in solution, the direct sequence of morphological transitions, S−C−L, is expected. We have constructed the scaling type diagrams of state of diblock copolymer solution and delineated the transition lines (binodals) that separate the stability regions of micelles with different morphologies. We demonstrated that due to weakly dissociating corona all micelle characteristics (aggregation number, interfacial area per chain, core radius, and corona thickness) exhibit nonmonotonic behavior upon variations in the solution salinity.

The nonmonotonic evolution of a micelle with pH-sensitive corona is attributed to the aggregation/ionization coupling. An increase in the solution salinity gives rise to two competing effects: enhancement of corona ionization and screening of the Coulomb repulsion between coronal chains. The former effect is dominant at low salt concentration, whereas the latter becomes significant at high salt concentration, when the coronal chains have already reached maximal degree of ionization $\alpha = \alpha_b$. Therefore, the strength of repulsive interaction between the coronal chains varies nonmonotonically as a function of salt concentration and is maximal in the intermediate range of salt concentrations. As a result, the aggregation number exhibits here a minimum.

Remarkably this behavior is different from that for diblock copolymer with a quenched (strongly dissociating) polyelectrolyte block or a conventional ionic surfactant. In a strongly dissociating polyelectrolyte the degree of ionization is constant and an increase in solution salinity results in the monotonic decrease in strength of the Coulomb repulsion between the coronal blocks. As a result, the aggregation number gradually increases due to enhanced screening of the electrostatic interaction in the corona. At low salt concentration the morphology of aggregates formed by strongly dissociating block polyelectrolytes is determined solely by the copolymer composition. We analyze the thermodynamic stability of different morphologies of such diblock copolymer in Appendix 3. (This analysis is complementary to our previous study, ref 22, where the morphologies of aggregates formed by the quenched block polyelectrolyte in the salt dominance limit were examined.)

Our theory is based on a number of assumptions. The strong stretching and the local electroneutrality approximations were implemented to describe the structure of micelle. We also assumed that the free ends of corona blocks are fixed at the outer boundary of the corona. A more refined self-consistent-field numerical model[25] indicates however that these approximations are not crucial to capture the basis physics of the system. The quantitative comparison between the results of the two models is in progress.

The experimental test of our predictions is a challenging problem. Equilibration of the micelle is a key point in the study of micelle rearrangement and the search for "direct" S−C−L and "reversed" L−C−S morphological transitions. A number of experimental studies[4,8,34] that focus on nanoaggregates in aqueous media deal with poly(styrene)-*block*-poly(acrylic acid)

copolymer. PS-*b*-PAA has a weakly dissociating acidic block with p$K \approx 5$, and its chemical composition can be varied. However, this block copolymer is hardly a suitable candidate to check our model. Polystyrene is known to become glassy in the micellar core and to prohibit equilibrium rearrangement of the micelle. Therefore, the aggregates of PS-*b*-PAA provide diverse model systems to study polymer brushes with fixed grafting density (corona of a micelle with the "frozen" core). For equilibrium micelles, a block copolymer with "softer" hydrophobic block, e.g., polyisobutylene or poly(*n*-butyl acrylate) are desirable.

We note that our model does not specify the state of solution with lamellar aggregates. Whereas thermodynamically stable individual neutral cylindrical micelles were found in dilute block copolymer solution,[33] lamellar aggregates tend to associate into a mesophase in sediment. Recent findings[34] on dispersed PS-*b*-PAA lamellar sheets indicated the existence of lamellar mesophase surrounded by pure water. Although the lamellar aggregates were clearly nonequilibrium due to a glassy PS core, the overall effect would be the same for the equilibrated lamellar bilayers. Because of planar geometry of the lamellar sheet, the attractive van der Waals forces are large enough to keep the lamellas together without noticeable perturbation of the corona.[33,34] Therefore, regions $L_{cc/qn}$, $L_{cc/osm}$, and $L_{cc/salt}$ in the phase diagram in Figure 5 correspond not to a homogeneous solution of individual dispersed lamellas but to a lamellar mesophase in sediment. The L−C binodals are then delineate the boundary between the homogeneous micellar solution and the solution segregated into a lamellar mesophase and water.

Acknowledgment. This work has been partially supported by the Dutch National Science Foundation (NWO) program "Computational approaches for multiscale modeling in self-organizing polymer and lipid systems", No 047.016.004, by the Russian Foundation for Basic Research (Grant 02-03-33127), and by the EUROCORES program within the project "Higher levels of Self-Assembly of Ionic Amphiphilic Copolymers" (SONS-AMPHI).

Appendix 1. Starlike Spherical Micelle

We consider a spherical micelle in the neutral and the salt dominance regimes. In both cases, the interactions in the corona are governed by binary monomer−monomer interactions with the second virial coefficient $v = v_A$ or $v = v_A + \alpha_b^2/2\Phi_{ion}$, respectively. The degree of ionization is uniform throughout the corona, $\alpha = 0$ and $\alpha = \alpha_b$ in the two respective regimes.

We start with the reference system, a planar brush with area $s = s(R)$ per chain. The free energy $F^{(1)}$ of a planar brush is given by

$$\frac{F^{(1)}}{k_B T} = N_A v c_p + \frac{3H^{(1)2}}{2N_A} + N_A \ln(1-\alpha) = N_A v c_p + \frac{3N_A}{2c_p^2 s^2} + N_A \ln(1-\alpha) \quad \text{(A1.1)}$$

where $c_p = N_A/sH^{(1)}$ is the concentration of monomers in the brush, $H^{(1)}$ is brush thickness, and $\alpha = 0$ or $\alpha = \alpha_b$. The first term in eq A1.1 accounts for the binary contacts between monomers ($\sim c_p$), and the second term describes elastic stretching of the chains ($\sim c_p^{-2}$), whereas the third term is constant, independent of c_p. By minimizing $F^{(1)}$with respect to c_p we find equilibrium characteristics of the planar brush

$$c_p^{(1)} = \left(\frac{3}{vs^2}\right)^{1/3} \quad \text{(A1.2)}$$

$$H^{(1)} = \frac{1}{3^{1/3}} N_A v^{1/3} s^{-1/3} \quad \text{(A1.3)}$$

$$\frac{F^{(1)}}{kT} = \frac{3^{4/3}}{2} N_A v^{2/3} s^{-2/3} + \ln(1-\alpha) \quad \text{(A1.4)}$$

The density of free energy in the spherical corona of micelle is given by

$$f\{c_p(r)\} = v c_p(r)^2 + \frac{3}{2c_p(r)s^2}\left(\frac{R}{r}\right)^4 + c_p(r)\ln(1-\alpha) \quad \text{(A1.5)}$$

where R is the radius of the core, and $\alpha = \text{const}(r)$ is already specified above.

The polymer density profile $c_p(r)$ is determined by eq 18 as

$$2v c_p(r) - \frac{3}{2c_p(r)^2 s^2}\left(\frac{R}{r}\right)^4 + \ln(1-\alpha) = \lambda \quad \text{(A1.6)}$$

or, equivalently

$$2v c_p(r) - \frac{3}{2c_p(r)^2 s^2}\left(\frac{R}{r}\right)^4 = 2v c_p(D) - \frac{3}{2c_p(D)^2 s^2}\left(\frac{R}{D}\right)^4 \quad \text{(A1.7)}$$

where $c_p(D)$ is the polymer density at the edge of the corona, $r = D$. Applying boundary condition, eq 19,

$$v c_p(D)^2 - \frac{3}{c_p(D)s^2}\left(\frac{R}{D}\right)^4 = 0 \quad \text{(A1.8)}$$

we find the value of $c_p(D)$:

$$c_p(D) = \left(\frac{3}{vs^2}\right)^{1/3}\left(\frac{R}{D}\right)^{4/3} = c_p^{(1)}\left(\frac{R}{D}\right)^{4/3} \quad \text{(A1.9)}$$

Introducing distance $z = r/D$ and reduced polymer density profile $y = c_p(r)/c_p(D)$, and using eq A1.9, we rewrite eq A1.7 as

$$4y - \frac{1}{y^2 z^4} = 3 \quad \text{(A1.10)}$$

or, equivalently,

$$z = \frac{1}{y^{1/2}(4y-3)^{1/4}} \quad \text{(A1.11)}$$

The equilibrium density of free energy in the corona is obtained from eqs A1.5, A1.9, A1.10 as

$$f\{y(r)\} = \frac{3}{2} v c_p(D)^2 y(2y-1) + c_p(D) y \ln(1-\alpha) \quad \text{(A1.12)}$$

The coronal free energy F_{corona} yields

$$F_{corona} = s\int_R^D f\{c_p(r)\}\left(\frac{r}{R}\right)^2 dr = s\frac{D^3}{R^2}\int_{R/D}^1 f\{y(r)\}z^2\, dz \quad \text{(A1.13)}$$

Changing integration variable z to y, calculating (dz/dy) from eq A1.11, and using eqs A1.4 and A1.3, we present F_{corona} as

$$\frac{F_{corona} - N_A \ln(1-\alpha_b)}{F^{(1)} - N_A \ln(1-\alpha_b)} = \frac{3R}{2H^{(1)}}\left(1+\frac{H}{R}\right)^{1/3}\int_1^{y_R}\frac{(2y-1)^2\, dy}{y^{3/2}(4y-3)^{7/4}} \quad \text{(A1.14)}$$

where $H = D - R$ is the corona thickness and y_R is the root of equation A1.10 at $z = R/D$. Similarly, normalization condition 17 can be re-formulated as

$$1 = \frac{3R}{2H^{(1)}}\left(1+\frac{H}{R}\right)^{5/3}\int_1^{y_R}\frac{(2y-1)\, dy}{y^{3/2}(4y-3)^{7/4}} \quad \text{(A1.15)}$$

Equations A1.14 and A1.15 are valid at arbitrary radii R and D of the core and of the corona, respectively. They can be simplified in the limit of starlike corona when $H/R \to \infty$ and $y_R \to \infty$. In this limit, eqs A1.14 and A1.15 reduce to

$$\frac{F_{corona} - N_A \ln(1-\alpha)}{F^{(1)} - N_A \ln(1-\alpha)} = \frac{3R}{2H^{(1)}}\left(\frac{H}{R}\right)^{1/3}\int_1^{\infty}\frac{(2y-1)^2\, dy}{y^{3/2}(4y-3)^{7/4}} = \frac{3R}{2H^{(1)}}\left(\frac{H}{R}\right)^{1/3}J_2 \quad \text{(A1.16)}$$

$$1 = \frac{3R}{2H^{(1)}}\left(\frac{H}{R}\right)^{5/3}\int_1^{\infty}\frac{(2y-1)\, dy}{y^{3/2}(4y-3)^{7/4}} = \frac{3R}{2H^{(1)}}\left(\frac{H}{R}\right)^{5/3}J_1 \quad \text{(A1.17)}$$

Here, the integrals J_1 and J_2 can be expressed in terms of special functions and calculated as

$$J_1 = 2B(2, 5/4)F(7/4, 2;13/4; -3) + B(1, 9/4)F(7/4, 1;13/4; -3) \approx 0.325$$

and

$$J_2 = 4B(2, 1/4)F(7/4, 2;9/4; -3) + B(1, 5/4)F(7/4, 1;9/4; -3) \approx 1.697$$

where $B(x, y)$ is the β function and $F(\alpha,\beta;\gamma;x)$ is the Gauss hypergeometric series.[35] Equations A1.16 and A1.17 provide the asymptotic dependences for corona thickness H and corona free energy F_{corona} in a starlike spherical micelle as a function of area $s(R)$ per chain, degree of polymerization N_A, second virial coefficient v, and core radius R:

$$\frac{H}{R} \approx \left(\frac{2}{3J_1}\frac{H^{(1)}}{R}\right)^{3/5} \quad \text{(A1.18)}$$

$$\frac{F_{corona} - N_A \ln(1-\alpha_b)}{F^{(1)} - N_A \ln(1-\alpha_b)} \approx \frac{3J_2}{2}\left(\frac{2}{3J_1}\right)^{1/5}\left(\frac{R}{H^{(1)}}\right)^{4/5} \quad \text{(A1.19)}$$

Equation A1.18 leads to

$$H \approx \frac{2^{1/5}}{3^{4/5}\pi^{1/5}J_1^{3/5}}N_A^{3/5}v^{1/5}p^{1/5}$$

where $p = 4\pi R^2/s(R)$ is the total number of chains in the corona.

By substituting $R = 3N_B/\tau s$ (eq 6), $F^{(1)}_{corona}$ (eqs A1.3), and $H^{(1)}$ (eq A1.4) in eq A1.19, we obtain the final expression for the free energy of a starlike corona

$$F_{corona}/k_BT \approx \frac{J_2}{J_1^{1/5}}\frac{3^{16/5}}{2^{9/5}}N_A^{1/5}N_B^{4/5}\tau^{-4/5}v^{2/5}s^{-6/5} + N_A\ln(1-\alpha) \quad \text{(A1.20)}$$

where $\alpha = 0$ and $\alpha = \alpha_b$ in the neutral and the salt dominance regimes, respectively. By minimizing total free energy per chain $F = F_{interface} + F_{corona}$ with respect to area s, we find the equilibrium characteristics of a starlike micelle. The results are presented in the text.

Appendix 2. Linear in Curvature Correction to the Free Energy of a Planar Brush

The free energy of corona in micelle of morphology i yields

$$F^{(i)}_{corona} = s(R)\int_R^D f\{c_p(r)\}\left(\frac{r}{R}\right)^{i-1} dr \quad \text{(A2.1)}$$

where corona radius D is determined by the condition

$$N_A = s(R)\int_R^D c_p(r)\left(\frac{r}{R}\right)^{i-1} dr \quad \text{(A2.2)}$$

By introducing corona thickness $H = D - R \ll R$ and new variable $z = D - r$, we represent eqs A2.1 and A2.2 as

$$F^{(i)}_{corona} = s(R)\left(\frac{D}{R}\right)^{i-1}\int_0^H f\{c_p(D-z)\}\left(1-\frac{z}{D}\right)^{i-1} dz = s(D)\int_0^H f\{c_p(D-z)\}\left(1-\frac{z}{D}\right)^{i-1} dz \quad \text{(A2.3)}$$

and

$$N_A = s(D)\int_0^H c_p(D-z)\left(1-\frac{z}{D}\right)^{i-1} dz \quad \text{(A2.4)}$$

Expansion of density of the free energy $f\{c_p(D-z)\}$ and of polymer density profile $c_p(D-z)$ in power series with respect to z in eqs A2.3 and A2.4 leads to

$$F^{(i)}_{corona} = s(D)\int_0^H\left[f\{c_p(D)\} - z\left(\frac{df\{c_p(r)\}}{dr}\right)_D + ...\right]\left[1 - (i-1)\frac{z}{D} + ...\right] dz \quad \text{(A2.5)}$$

and

$$N_A = s(D)\int_0^H\left[c_p(D) - z\left(\frac{dc_p}{dr}\right)_D + ...\right]\left[1 - (i-1)\frac{z}{D} + ...\right] dz \quad \text{(A2.6)}$$

where $s(D) = s(R)(D/R)^{(i-1)}$ is the area per chain at the edge of the corona, i.e., at $r = D$. By retaining only the

terms linear in z and performing integration in eqs A2.5 and A2.6, we obtain

$$F^{(i)}_{\text{corona}} \approx s(D)\left[f\{c_p(D)\}H - \frac{H^2}{2D}\left[(i-1)f\{c_p(D)\} + \left(\frac{df\{c_p(r)\}}{dr}\right)_D D\right] = s(D)f\{c_p(D)\}H\left\{1 - \frac{H}{2D}\left[(i-1) + \left(\frac{df\{c_p(r)\}}{dr}\right)_D \frac{D}{f\{c_p(D)\}}\right]\right\} \quad \text{(A2.7)}$$

and

$$N_A \approx s(D)\left[c_p(D)H - \frac{H^2}{2D}\left[(i-1)c_p(D) + \left(\frac{dc_p}{dr}\right)_D D\right] = s(D)c_p(D)H\left\{1 - \frac{H}{2D}\left[(i-1) + \left(\frac{dc_p}{dr}\right)_D \frac{D}{c_p(D)}\right]\right\} \quad \text{(A2.8)}$$

We introduce thickness of planar brush $H^{(1)}_D \equiv H\{s(D)\}$ and free energy $F^{(1)}_D \equiv F\{s(D)\}$ of a planar brush with area $s(D)$ per chain as

$$N_A = H^{(1)}_D c_p(D) s(D) \quad \text{(A2.9)}$$

and

$$F^{(1)}_D = f\{c_p(D)\}s(D)H^{(1)}_D \quad \text{(A2.10)}$$

Equations A2.7 and A2.8 are then presented as

$$F^{(i)}_{\text{corona}} = F^{(1)}_D \frac{H}{H^{(1)}_D}\left\{1 - \frac{H}{2D}\left[(i-1) + \left(\frac{df\{c_p(r)\}}{dr}\right)_D \frac{D}{f\{c_p(D)\}}\right]\right\} \quad \text{(A2.11)}$$

$$1 = \frac{H}{H^{(1)}_D}\left\{1 - \frac{H}{2D}\left[(i-1) + \left(\frac{dc_p}{dr}\right)_D \frac{D}{c_p(D)}\right]\right\} \quad \text{(A2.12)}$$

By dividing eq A2.11 by eq A2.12, we find

$$F^{(i)}_{\text{corona}} = F^{(1)}_D\left\{1 - \frac{H}{2D}\left[\left(\frac{df\{c_p(r)\}}{dr}\right)_D \frac{D}{f\{c_p(D)\}} - \left(\frac{dc_p}{dr}\right)_D \frac{D}{c_p(D)}\right]\right\} \quad \text{(A2.13)}$$

The term in square brackets in eq A2.13 can be simplified by representing df/dr as

$$\frac{df\{c_p(r)\}}{dr} = \frac{\delta f\{c_p(r)\}}{\delta c_p(r)}\frac{dc_p(r)}{dr} + \frac{\partial f\{c_p(r)\}}{\partial r} \quad \text{(A2.14)}$$

Here, (df/dr) is full derivative, $(\delta f/\delta c)$ is variational derivative, and $(\partial f/\partial r)$ is partial derivative of $f\{c_p(r)\}$. By substituting eq A2.14 in eq A2.13, and using the boundary condition, eq 19, we find

$$F^{(i)}_{\text{corona}} = F^{(1)}_D\left\{1 - \frac{H}{2D}\left[\left(\frac{\partial f\{c_p(r)\}}{\partial r}\right)_D \frac{D}{f\{c_p(D)\}}\right]\right\} \quad \text{(A2.15)}$$

Density of the free energy $f\{c_p(r)\}$ in the corona (eq 15) can be presented as

$$f\{c_p(r)\} = f_{\text{int}}\{c_p(r)\} + f_{\text{elastic}}\{c_p(r)\} = f_{\text{int}}\{c_p(r)\} + \frac{3}{2c_p(r)s^2}\left(\frac{R}{r}\right)^{2(i-1)} \quad \text{(A2.16)}$$

where $f_{\text{int}}\{c_p(r)\}$ accounts for monomer−monomer interactions and depends only on local polymer density $c_p(r)$, whereas elastic contribution $f_{\text{elastic}}\{c_p(r)\}$ is specified by both, $c_p(r)$ and r. Therefore,

$$D\left(\frac{\partial f\{c_p(r)\}}{\partial r}\right)_D = D\left(\frac{\partial f_{\text{elastic}}\{c_p(r)\}}{\partial r}\right)_D = -2(i-1)\frac{3}{2c_p(r)s^2}\left(\frac{R}{D}\right)^{2(i-1)} \quad \text{(A2.17)}$$

and eq A2.15 reduces to

$$F^{(i)}_{\text{corona}} = F^{(1)}_D\left\{1 + (i-1)\frac{H}{D}\left(\frac{f_{\text{elastic}}\{c_p(D)\}}{f\{c_p(D)\}}\right)\right\} \quad \text{(A2.18)}$$

Free energy $F^{(1)}_D \equiv F^{(1)}\{s(D)\}$ can be also expanded as

$$F^{(1)}\{s(D)\} = F^{(1)}\{s(R)\} + \left(\frac{dF^{(1)}}{ds}\right)_R\left(\frac{ds}{dr}\right)_R (D-R) + \ldots = F^{(1)}\{s(R)\}\left\{1 + (i-1)\frac{H}{R}\left(\frac{dF^{(1)}}{ds}\right)\frac{s}{F^{(1)}\{s(R)\}}\right\} \quad \text{(A2.19)}$$

where (ds/dr) is calculated from eq 6. Let $H\{s(R)\} \equiv H^{(1)}_R$ and $F\{s(R)\} \equiv F^{(1)}_R$ be the thickness and the free energy of a planar brush with grafting area $s = s(R)$. With accuracy of linear in curvature terms, eqs A2.18 and A2.19 give

$$F^{(i)}_{\text{corona}} = F^{(1)}_R\left\{1 + (i-1)\frac{H^{(1)}_R}{R}\left[\left(\frac{dF^{(1)}}{ds}\right)_R \frac{s}{F^{(1)}_R} + \frac{f_{\text{elastic}}\{c_p(R)\}}{f\{c_p(R)\}}\right]\right\} = F^{(1)}\left\{1 + (i-1)\frac{H^{(1)}_R}{R}\left[\left(\frac{dF^{(1)}}{ds}\right)_R \frac{s}{F^{(1)}_R} + \frac{F^{(1)}_{\text{elastic}}\{s(R)\}}{F^{(1)}_R}\right]\right\} \quad \text{(A2.20)}$$

Here

$$F^{(1)}_{\text{elastic}} = N_A f_{\text{elastic}}\{c_p(R)\}/c_p(R) = 3N_A c_p(R)^{-2}s^{-2}$$

and

$$F^{(1)}_R = N_A f\{c_p(R)\}/c_p(R)$$

are the elastic and the total free energy of a planar brush with area $s = s(R)$. Taking advantage of equality

$$\frac{dF^{(1)}}{ds} = \frac{\partial F^{(1)}}{\partial s} + \frac{\partial F^{(1)}}{\partial c_p}\frac{\partial c_p}{\partial s} \quad \text{(A2.21)}$$

where $c_p(s) = N_A/sH^{(1)}(s)$, using the condition of equilibrium in the planar brush, $\partial F^{(1)}/\partial c_p = 0$, and dif-

ferentiating, $s\partial F^{(1)}/\partial s = -2F^{(1)}_{\text{elastic}}$, we finally obtain

$$F^{(i)}_{\text{corona}} = F^{(1)}_R\left\{1 - (i-1)\frac{H^{(1)}_R}{R}\frac{F^{(1)}_{\text{elastic}}\{s(R)\}}{F^{(1)}_R}\right\} = F^{(1)}_R - (i-1)\frac{3H^{(1)3}_R}{2RN_A} \quad \text{(A2.22)}$$

Equation A2.22 indicates that with accuracy of linear in curvature terms, the change in the free energy due to corona bending, $(F^{(i)}_{\text{corona}} - F^{(1)}_R)$, is determined by thickness $H^{(1)}_R$ of the planar brush and corona morphology i. Equation A2.22 was obtained under assumption of the Gaussian elasticity for the tethered chains and arbitrary functional form of interaction free energy $f_{\text{int}}\{c_p(r)\}$.

Appendix 3

In this appendix, we consider the ranges of thermodynamic stability for micellar aggregates of different morphologies formed by diblock copolymer with quenched polyelectrolyte block in the salt free solution. In this case only counterions ensuring the total electroneutrality of the system are present, and the local electroneutrality condition is given by

$$\alpha_b c_p(r) = c_+(r) \quad \text{(A3.1)}$$

Here, α_b is the constant (quenched) degree of ionization of the coronal block.

The free energy density in the corona yields

$$f\{c_p(r)\}/k_BT = \frac{3}{2c_p(r)s^2(r)} + v_A c_p^2(r) + \alpha_b c_p(r)[\ln(\alpha_b c_p(r)) - 1] \quad \text{(A3.2)}$$

where the last term accounts for the translational entropy of counterions.

By using eq 30, we obtain the free energy of the corona in the crew cut limit ($D - R \ll R$) with the accuracy up to linear in curvature terms,

$$F^{(i)}_{\text{corona}}/k_BT \approx F^{(1)}_{\text{corona}}/k_BT - \frac{(i-1)}{2\sqrt{3}}\frac{\alpha_b^{3/2}N_A^2 s(R)\tau}{N_B} \quad \text{(A3.3)}$$

where

$$F^{(1)}_{\text{corona}}/k_BT = \alpha_b N_A\left[\ln\frac{\sqrt{3\alpha_b}}{s(R)} - \frac{1}{2}\right] \quad \text{(A3.4)}$$

Balance of the first term in eq *A*3.3 and the interface free energy, eq 5, gives $s \cong \alpha_b N_A/\gamma$. The total free energy per chain in the micelle yields

$$F^{(i)}/k_BT \approx F^{(1)}/k_BT - \frac{(i-1)}{2\sqrt{3}i}\frac{\alpha_b^{5/2}N_A^3\tau}{\gamma N_B} + b_i\frac{i^2N_B\gamma^2}{\tau^2\alpha_b^2N_A^2} \quad \text{(A3.5)}$$

The binodal line separating the regions of thermodynamic stability of aggregates of morphology i and $i+1$ is given by

$$\frac{\alpha_b^{9/2}N_A^5\tau^3}{N_B^2\gamma^3} = 2\sqrt{3}[i(i+1)[(i+1)^2b_{i+1} - i^2b_i]], \quad i = 1, 2 \quad \text{(A3.6)}$$

The transition from morphology i to $i+1$ (i.e., lamella−cylinder or cylinder−sphere) occurs upon an increase in the degree of ionization of the coronal blocks α_b or/and an increase in N_A/decrease in N_B.

References and Notes

(1) Tanford, C. *The Hydrophobic Effect: Formation of Micelles and Biological Membranes,*Wiley-Interscience: New York, 1973.
(2) Israelachvili J. N. *Intermolecular and Surface Forces*, Academic Press: London, 1985.
(3) Kiserow, D.; Prochazka, K.; Ramireddy, C.; Tuzar, Z.; Munk, P.; Webber, S. E. *Macromolecules* **1992**, *25*, 461.
(4) (a) Zhung, L.; Eisenberg, A. *Science* **1995**, *268*, 1728. (b) Khougaz, K.; Astafieva, I.; Eisenberg, A. *Macromolecules* **1995**, *28*, 7135.
(5) Amiel, C.; Sikka, M.; Schneider, J. W.; Tsao, Y. H.; Tirrell, M.; Mays, J. W. *Macromolecules* **1995**, *28*, 3125.
(6) (a) Guenoun, P.; Delsanti, M.; Gaseau, D.; Auvray, L.; Cook, D. C.; Mays, J. W.; Tirrell, M. *Eur. Phys. J. B* **1998**, *1*, 77. (b) Guenoun, P.; Davis, H. T.; Tirrell, M.; Mays, J. W. *Macromolecules* **1996**, *29*, 3965. (c) Guenoun, P.; Muller, F.; Delsanti, M.; Auvray, L.; Chen, Y. J. Mays, J. W.; Tirrell, M. *Phys. Rev. Lett.* **1998**, *81*, 3872. (d) Muller, F.; Delsanti, M.; Auvray, L.; Yang, J.; Chen, Y. J.; Mays, J. W.; Demé, B.; Tirrell, M.; Guenoun, P. *Eur. Phys. J. E* **2000**, *3*, 45.
(7) Förster, S.; Hemsdorf, N.; Leube, W.; Schnablegger, H.; Regenbrecht, M.; Akari, S.; Lindner, P.; Böttcher, C. *J. Phys. Chem.* **1999**, *103*, 6657.
(8) (a) Groenewegen, W.; Egelhaalf, S. U.; Lapp, A.; van der Maarel, J. R. C. *Macromolecules* **2000**, *33*, 3283. (b) Groenewegen, W.; Lapp, A.; Egelhaalf, S. U.; van der Maarel, J. R. C. *Macromolecules* **2000**, *33*, 4080.
(9) Schuch, H.; Klingler, J.; Rossmanith, P.; Frechen, T.; Gerst, M.; Feldthusen, J.; Müller, A. H. E. *Macromolecules* **2000**, *33*, 3687.
(10) Förster, S.; Hermsdorf, N.; Böttcher, C.; Lindner, P. *Macromolecules* **2002**, *35*, 4096.
(11) (a) Krämer, E.; Förster, S.; Göltner, C.; Antonietti, M. *Langmuir* **1998**, *14*, 2027. (b) Regenbrecht, M.; Akari, S.; Förster, S.; Möhwald, H. *Surf. Interface Anal.* **1999**, *27*, 418.
(12) Förster, S.; Hermsdorf, N.; Leube, W.; Schnablegger, H.; Regenbrecht, M.; Akari, S.; Lindner, P.; Böttcher, C. *J. Phys. Chem. B* **1999**, *103*, 6652.
(13) Regenbrecht, M.; Akari, S.; Förster, S.; Möhwald, H. *J. Phys. Chem. B* **1999**, *103*, 6668.
(14) Regenbrecht, M.; Akari, S.; Förster, S.; Netz, R.R.; Möhwald, H. *Nanotechnology* **1999**, *10*, 434.
(15) Förster, S.; Abetz, V.; Müller A. H. E. *Adv. Polym. Sci.* **2004**, *166*, 173.
(16) Marko, J. F.; Rabin, Y. *Macromolecules* **1992**, *25*, 1503.
(17) Wittmer, J.; Joanny, J.-F. *Macromolecules* **1993**, *26*, 2691.
(18) Shusharina, N. P.; Nyrkova, I. A.; Khokhlov, A. R. *Macromolecules* **1996**, *29*, 3167.
(19) Huang, C.; Olivera de la Cruz, M.; Delsanti, M.; Guenoun, P. *Macromolecules* **1997**, *30*, 8019.
(20) Borisov, O. V.; Zhulina, E. B. *Macromolecules* **2002**, *35*, 4472.
(21) Zhulina, E. B.; Borisov, O. V. *Macromolecules* **2002**, *35*, 9191.
(22) Borisov, O. V.; Zhulina, E. B. *Macromolecules* **2003**, *36*, 10029.
(23) (a) Zhulina, E. B.; Birshtein, T. M. *Polym. Sci. USSR* **1985**, *27*, 570. (b) Halperin, A. *Macromolecules* **1987**, *20*, 2943. (c) Birshtein, T. M.; Zhulina, E. B. *Polymer* **1989**, *30*, 170. (d) Halperin, A. *Europhys. Lett.* **1989**, *8*, 351.
(24) Halperin, A. Polymeric vs Monomeric Amphiphiles: Design Parameters. In *Supramolecular Polymers*; Ciferri, A., Ed.; Marcel Dekker, New York, 2000.
(25) Lauw, Y.; Leermakers, F. A. M.; Cohen Stuart, M. A. Manuscript in preparation.

(26) Borisov, O. V.; Zhulina, E. B. *Langmuir*, in press.
(27) de Gennes, P. G. *Scaling Concepts in Polymer Physics*; Cornell University Press: Ithaca, NY, and London, 1979.
(28) Semenov, A. N. *Sov. Phys. JETP* **1985**, *61*, 733.
(29) Pincus, P. A. *Macromolecules* **1991**, *24*, 2912.
(30) (a) Zhulina E. B.; Birshtein, T. M.; Borisov O. V. *Macromolecules* **1995**, *28*, 1491. (b) Lyatskaya, Yu. V.; Leermakers, F. A. M.; Fleer, G. J.; Zhulina, E. B.; Birshtein, T. M. *Macromolecules* **1995**, *28*, 3562.
(31) Zhulina, E. B.; Borisov, O. V. *Macromolecules* **1996**, *29*, 2618.
(32) Note, that due to noticeable difference in v_A and $v = v_A + \alpha_b^2/2\Phi_{ion} \gg v_A$, the micelle free energy in the low salt regime (eq 23) is much smaller than the absolute value of each of the two contributions to the micelle free energy in the high salt regime, eq 24. Therefore, the approximate value of Φ^*_{ion} can be found from the condition $F^{(3)}_{highsalt} = 0$. By expanding the logarithmic term in 24 with respect to $\alpha_b < 1$, we find the scaling dependence for Φ^*_{ion}, eq 29.
(33) Zhulina, E. B.; Adam, M.; LaRue, I.; Sheiko, S.; Rubinstein, M. *Macromolecules* **2005**, in press.
(34) Bendejacq, D.; Ponsinet, V.; Joanicot, M. *Eur. Phys. J. E* **2004**, 1*3*, 3.
(35) Gradshteyn, I. S.; Ryzhik, I. M. *Tables of Integrals, Series, and Products. Fifth Edition*; Academic Press: San Diego, CA, 1994.

MA050634W